Climate Dynamics (2004) 23: 99–115
DOI 10.1007/s00382-004-0417-x

M-P. Girardin · J. Tardif · M. D. Flannigan
Y. Bergeron

Multicentury reconstruction of the Canadian Drought Code from eastern Canada and its relationship with paleoclimatic indices of atmospheric circulation

Received: 12 December 2002 / Accepted: 12 February 2004 / Published online: 13 July 2004

Abstract Inter-annual and -decadal scale variability in drought over the Abitibi Plains ecoregion (eastern Canada) was investigated using a 380-year dendroclimatic reconstruction of the Canadian Drought Code (CDC; July monthly average) i.e., a daily numerical rating of the average moisture content of deep organic layers. Spectral analyses conducted on the reconstructed CDC indicated a shift in spectral power after 1850 leading toward a reduction in interdecadal variability and an increase in interannual variability. Investigation on the causes for this shift suggested a decrease in North Pacific forcing after the mid-nineteenth century. Cross-continuous wavelet transformation analyses indicated coherency in the 8–16 and 17–32-year per cycle oscillation bands between the CDC reconstruction and the Pacific Decadal Oscillation (PDO) prior to 1850. Following 1850, the coherency shifted toward the North Atlantic Oscillation (NAO). Principal component analysis conducted over varying time windows reaffirmed that the Pacific forcing was restricted to the period about 1750–1850. Prior to and after this period, the CDC was correlated with the NAO. The shift around 1850 could reflect a northward displacement of the polar jet stream induced by a warming of the sea surface temperature along the North Pacific coast. A northward displacement of the jet stream, which inhibits the outflow of cold and dry Arctic air, could have allowed the incursion of air masses from the Atlantic subtropical regions.

M-P. Girardin (✉) · J. Tardif
Centre for Forest Interdisciplinary Research (C-FIR),
University of Winnipeg, 515 Avenue Portage, Winnipeg,
Manitoba, R3B 2E9, Canada
E-mail: m.girardin@uwinnipeg.ca

M. D. Flannigan
Canadian Forest Service, 1219 Queen St East,
Sault Ste Marie, Ontario P6A 2E5, Canada

M-P. Girardin · Y. Bergeron
Groupe de recherche en écologie forestière inter-universitaire
(GREFI), Université du Québec à Montréal,
C.P. 8888, Succ. Centre-Ville, Montréal,
Québec, H3C 3P8, Canada

M-P. Girardin
Department of Botany, University of Manitoba,
505 Buller Building, Winnipeg, Manitoba,
R3T 2N2, Canada

1 Introduction

Interactions between the oceans and the atmosphere can affect air mass circulation and climate over vast geographical areas (Minobe 1997; Nigam et al. 1999; Latif et al. 2000; Barlow et al. 2001; Bonsal et al. 2001). In North America, several investigations reported extreme weather events associated with anomalous sea surface temperatures (SST) or sea level pressures (SLP) across the Arctic, the Pacific, and the Atlantic sectors (Shabbar and Khandekar 1996; Hurrell and Van Loon 1997; Shabbar et al. 1997a, b; Thompson and Wallace 1998; Nigam et al. 1999; Barlow et al. 2001). These anomalies act by altering the atmospheric circulation patterns across the oceans, which subsequently influence temperature, precipitation and storm tracks over large land areas. These anomalies can typically last for weeks to several months, and in some cases they can persist for several years and decades (Rogers 1984; Ropelewski and Jones 1987; Bonsal et al. 1993; Hurrell 1995, 1996; Zhang et al. 1997).

There is substantial evidence of long-term changes in atmospheric circulation patterns across the Arctic, the Pacific, and the Atlantic sectors (Cook et al. 1998; Luterbacher et al. 1999, 2002; D'Arrigo et al. 2001; Glueck and Stockton 2001; Thompson and Wallace 2001). The contribution of anthropogenic forcing to recent Northern Hemisphere changes versus that of solar radiation, ozone depletion and volcanic aerosols is still being investigated (e.g. Gillett et al. 2002; Shindell et al. 2001a, b). Nevertheless, changes in atmospheric circulation may have affected the climate in eastern

Canada (Bergeron and Archambault 1993). Eastern Canada's climate is notably becoming moister (Bergeron and Archambault 1993; Tardif and Bergeron 1997a), despite global warming (Houghton et al. 2001). Instrumental climate records in eastern Canada effectively show an increase of annual mean temperature by 0.5 to 1.5 °C in the last 100 years, with a greater warming in minimum than maximum temperature (Vincent and Gullett 1999; Zhang et al. 2000). However, mean precipitation also has significantly increased and particularly the amount of snowfall received in spring (Mekis and Hogg 1999; Zhang et al. 2000). Climate simulation using general circulation models (GCMs) supported an increase in the frequency of precipitation under a $2 \times CO_2$ scenario (Bergeron and Flannigan 1995; Flannigan et al. 1998, 2001; Flannigan and Wotton 2001).

Paleo-climatological and -ecological investigations suggested that climate in eastern Canada started to change with the end of the 'Little Ice Age' (~1850). In the southeastern boreal forest, analysis of ice scars on flooded *Thuja occidentalis* L. trees indicated an increase in height and frequency of spring water levels at ice break-up since 1850 (Tardif and Bergeron 1997a). This increase in flood severity occurred in conjunction with a movement of *Fraxinus nigra* March. populations from low floodplain sites to more elevated sites along the flooding gradient (Tardif and Bergeron 1999). In addition, dendroecological reconstructions of stand dynamics revealed that *Thuja occidentalis* (a late successional species) became more abundant in the landscape after 1850 as a result of a decrease in fire frequency (Bergeron 1998, 2000, Bergeron et al. 2001). Many other studies reported changes in forest dynamics associated with climatic change across the boreal and the subarctic areas of eastern Canada (Morin and Payette 1984; Bégin and Payette 1988; Bégin et al. 1993; Hofgaard et al. 1999; Bégin 2000).

It was speculated that the poleward retreat of the Arctic air mass starting at the end of the 'Little Ice Age' contributed to the incursion of moister air masses in eastern Canada (Bergeron and Archambault 1993; Hofgaard et al. 1999). However, numerous indications suggest that a more complex change in climate dynamics occurred around 1850. In many tree-ring chronologies of eastern Canada, Hofgaard et al. (1999) observed an increase in mean sensitivity around 1850. This coincides with the shift in the power spectrum of paleoclimatic records from the Pacific (Stahle et al. 1998; D'Arrigo et al. 2001). Such a shift was not observed in paleoclimatic records of the North Atlantic (Cook et al. 1998; Glueck and Stockton 2001; Wanner et al. 2001; D'Arrigo et al. 2002).

The objective of this study was to (1) reconstruct past summer drought over the Abitibi Plains ecoregion, eastern Canada, and (2) analyze its relationships with climate variability of the North Pacific, tropical Pacific and North Atlantic between 1700 to present-day. First, a 380-year reconstruction of the July monthly average of the Canadian Drought Code (CDC; Van Wagner 1987) was developed from sixteen well-replicated residual tree-ring chronologies. Past studies have shown a good correlation between the CDC and ring width (Archambault and Bergeron 1992; Tardif and Bergeron 1997b; Girardin et al. 2001). The coherency between the reconstructed CDC and other climate reconstructions from the North Pacific (D'Arrigo et al. 2001), the tropical Pacific (Stahle et al. 1998) and the North Atlantic (Luterbacher et al. 1999) was analyzed. In addition, the CDC reconstruction was compared with records of fire history to test its ability to estimate past fire seasons. Since our record is an estimate of the average moisture content of the deep organic layers, it was expected that most periods of extensive burned area coincided with severe drought estimates.

2 Materials and methods

2.1 Description of the area

The study area (49°N, 79°W; approximately 125,664 km^2) is located at about 530 km north of Montreal and is part of the Northern Clay Belt of Québec and Ontario (Fig. 1). The geomorphology of the region is characterized by the influence of a post-glacial lacustrine phase that formed the Clay Belt (Vincent and Hardy 1977). The region is classified as having a humid mid-boreal ecoclimate (Ecological Stratification Working Group 1996). Mean annual temperature (1971–2000) at La Sarre is 0.7 °C, and total annual precipitation is 889.8 mm (Environment Canada 2002). The mean number of days with minimum temperature above 0 °C is 148. Snow represents 27.7% of the yearly total precipitation whereas most of the liquid precipitation falls during May to September (Environment Canada 2002). Human settlement mainly started in the 1910s, fire suppression started around the 1970s (Bergeron et al. 2001).

2.2 The Canadian drought code

The CDC is a numerical daily rating of the average moisture content of deep, compact, organic layers (Turner 1972). The CDC is a component of the Fire Weather Index System (Van Wagner 1987) that is used daily across Canada by the Canadian Forest Service (Natural Resources Canada) to monitor forest fire danger. In an ecological perspective, the CDC as many notable features : (1) the effect of snowmelt is accounted for in its calculation; (2) it is an adequate indicator of moisture conditions of deep organic layers in boreal conifer stands (Van Wagner 1970), (3) it represents conditions conducive to hydric stress in boreal tree species (Bergeron and Archambault 1993; Tardif and Bergeron 1997; Girardin et al. 2001), (4) it is an indicator of water table depth, and (5) it represents conditions conducive to fire involving deep soil layers (Turner

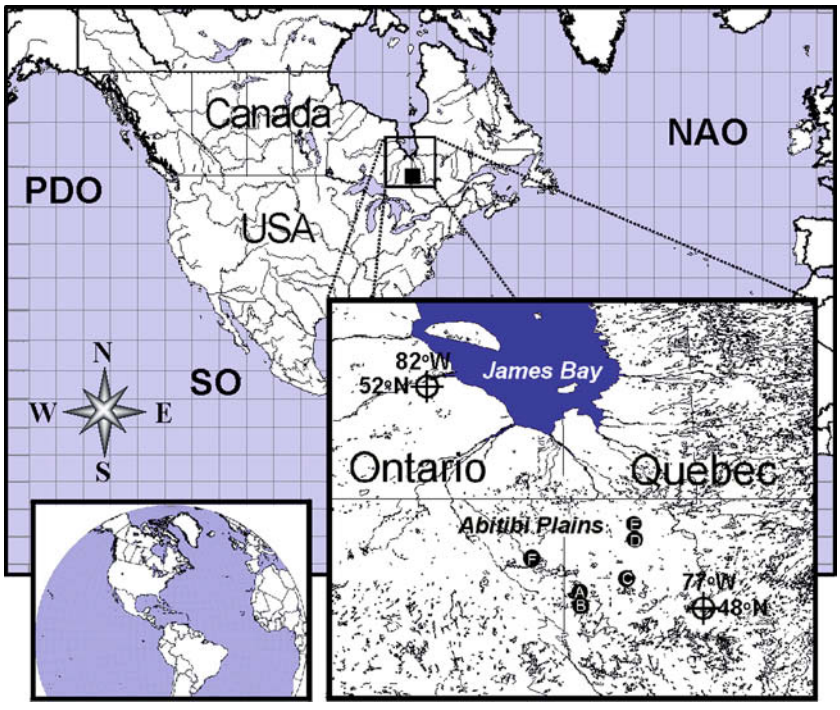

Fig. 1 Map showing the location of the study area. Geographical locations of the indices of climate variability over the Atlantic and Pacific sectors are shown, as well as the location of the tree-ring data sets (*A* 1, 5, 7, 12–16; *B* 8; *C* 3, 10; *D* 4, 11; *E* 2, 9; *F* 6, refer numbers to Table 1 for identification of chronologies)

1972). In addition, monthly CDC averages possess these statistical features: (a) the absence of serial autocorrelation in the monthly indices, (b) strong monthly persistence (high correlation between CDC indices from one month to the next), and (c) the presence of white noise in the CDC indices' spectra (decreasing power with increasing period) (Girardin et al. 2004).

The CDC maintains a daily budget of stored moisture, accounting for daily losses and gains (McAlpine 1990). The CDC is calculated each year independently of the previous one and of the amount of winter precipitation. Each year a snowmelt time is simulated (usually around May 1st in the eastern boreal forest). At that moment it is assumed that deep organic layers are fully recharged with water (as a consequence of melting snow). Thereafter, moisture losses are the result of daily evaporation and transpiration, while daily precipitation accounts for moisture gains (see Appendix 1). Evaporation and transpiration losses are first estimated as a maximum potential evapotranspiration based on temperature and date. Second, this maximum potential evapotranspiration value is scaled by the available soil moisture to reflect the fact that as soil moisture content is reduced, evaporation is increasingly difficult (Turner 1972; McAlpine 1990). In the moisture recharge procedure, total precipitation is reduced by 2.8 mm per 24 h period to allow for canopy and surface fuel interception. The maximum water holding capacity of the CDC is 100 mm for a layer with a bulk density of about 25 kg/m^2, which amounts to approximately 400% of water per units of mass. Excess water is considered as runoff and not accounted for in the CDC.

The minimum CDC value of zero represents 20.32 cm of available water held in the soil. The scale of the CDC is cumulative, with each unit change representing a decrease of 0.254 mm of available water in the soil. Van Wagner (1970) estimated the CDC exponential drying rate time constant at 52 days. A CDC rating of 200 is an indication of high drought severity, and 300 or more is extreme drought severity. The CDC generally peaks in mid- to late August, where afterward it either declines or maintains the same value (McAlpine 1990; Girardin et al. 2004). The reversal in August is only attributed to a change in day length, and is not a function of seasonal precipitation.

Daily CDC indices were computed using daily maximum temperature and daily precipitation data for each of the following stations: Amos, Abitibi Post, Cochrane, Duparquet, Haileybury, Kirkland, Iroquois Falls, La Sarre, and Val St-Gilles (data from Environment Canada 2000). Monthly average CDC indices of all stations were tested for homogeneity (Vincent 1998; program HOM, Holmes 1999) and a regional monthly CDC value was calculated using program MET (Holmes 1999). In this procedure, the mean and standard deviation was calculated for each month at each station. The departure for each month and year was then calculated and averaged across stations to produce regional average departures for each month and year.

2.3 Dendrochronological data

Sixteen well replicated tree-ring chronologies (a total of 1,191 measurement series) all greater than 170 years were obtained for reconstruction of the July CDC. These site chronologies are briefly described in Table 1. Most

Table 1 Residual tree-ring chronologies sources and main characteristics of each reconstruction model

Species	Source	Location	Length	N series total	$r(y)$	$r(y–1)$	Models				
							I	II	III	IV	V
01-*Pinus banksiana*	Hofgaard et al. (1999)	Hébécourt Lake	219	49	–0.38	–0.12	[a]				
02-*Pinus banksiana*	Hofgaard et al. (1999)	Chicobi Hills	182	57	–0.13	–0.28	[a]				
03-*Pinus banksiana*	Hofgaard et al. (1999)	Hedge Hills	185	67	–0.08	–0.01	[a]				
04-*Pinus banksiana*	Hofgaard et al. (1999)	Joutel	282	51	0.11	–0.27	[a]	[a]	[a]		
05-*Pinus banksiana*	Bergeron et al. (2001)	Duparquet Lake	260	94	–0.38	–0.09	[a]	[a]			
06-*Pinus banksiana*	Bergeron et al. (2001)	Abitibi Lake	275	75	–0.02	–0.29	[a]	[a]			
07-*Picea mariana*	Hofgaard et al. (1999)	Hébécourt Lake	206	59	–0.33	–0.18	[a]				
08-*Picea mariana*	Hofgaard et al. (1999)	Opasatica Lake	298	61	–0.25	–0.23	[a]	[a]	[a]		
09-*Picea mariana*	Hofgaard et al. (1999)	Chicobi Hills	177	61	–0.28	–0.24	[a]				
10-*Picea mariana*	Hofgaard et al. (1999)	Hedge Hills	181	67	–0.32	–0.04	[a]				
11-*Picea mariana*	Hofgaard et al. (1999)	Joutel	218	57	0.03	–0.23	[a]				
12-*Thuja occidentalis*	Archambault and Bergeron (1992)	Duparquet Lake	802	55	–0.32	–0.16	[a]	[a]	[a]	[b]	[b]
13-*Thuja occidentalis*	Tardif and Bergeron (1997b)	Duparquet Lake (wet sites)	571	43	–0.13	–0.12	[a]	[a]	[a]	[b]	[b]
14-*Fraxinus nigra*	Tardif and Bergeron (1997b)	Duparquet Lake (mesic sites)	308	253	–0.27	0.14	[a]	[a]	[a]		
15-*Picea mariana*	Girardin et al. (2001; 2002a)	Duparquet Lake (wet sites)	166	68	–0.15	–0.16	[a]				
16-*Betula papyrifera*	Charron and Bergeron (2000)	Duparquet Lake	233	74	–0.46	0.13	[a]	[a]			
Characteristics											
Length of the spline curves							60	60	60	60	300
Number of PCs used in the calibrations							2	2	2	4	4

Models: (I) 1820–1984; (II) 1768–1984; (III) 1714–1984; (IV-V) 1605–1984

[a]: residual chronologies used in the models

[b]: residual series used in the models

r: Pearson's correlation coefficients between the chronologies and the July instrumental CDC index (period 1895–1985) of the current year (y) of ring formation and the year prior ($y–1$) to ring formation. A correlation is significant at $P < 0.05$ when $r > |0.21|$

of these chronologies originated from the Lake Duparquet and surrounding areas (Fig. 1).

The site residual chronologies were created as follows. During sampling years, cores and cross sections were taken from trees. Cross sections were also taken from dead trees. The collected samples were sanded, crossdated, and each annual ring was measured at 0.001 mm accuracy (Stokes and Smiley 1996). For each measurement series, the crossdating was statistically verified using the program COFECHA (Holmes et al. 1986) and graphically using program ITRVIEW 2.0 (Varem-Sanders 2000). The age/size-related trend was removed from the tree-ring measurement series using a spline function giving a 50% oscillation response of 60 years (Cook and Peters 1981). Although this resulted in the loss of information relative to long-term climatic changes, 99% of the variance contained in oscillations less than 19 years was preserved. This "flexible" smoothing was necessary because many of the tree-ring series were less than a 100-year length, presenting important growth trends that needed to be removed. The biological persistence (autocorrelation) contained in the standardized measurement series was removed (autoregressive modeling) to eliminate variation not due to climate (Cook and Holmes 1986; Holmes et al. 1986). Biweight means of these residual series were computed for each data set to create the site residual chronologies. All chronologies were constructed using Program ARSTAN (Holmes 1999).

2.4 Subset models

The July CDC reconstruction was made from varying site residual chronologies and residual series. In this procedure, four sub-reconstruction models were created: model I (1820–1984), model II (1768–1984), model III (1714–1984), and model IV (1605–1984). The difference between models I, II, and III relates to the number of site residual chronologies included (16, 8, and 5, respectively; Table 1). Model IV was made from 39 long residual series greater than 380 years extracted from the two *Thuja occidentalis* data sets (Table 1). Segments of models I (1820–1989), II (1768–1819), III (1714–1767), and IV (1605–1713) were joined into one single 380-year time series. Because of the flexible smoothing performed on the measurement series, a fifth reconstruction model (model V) was made for assessment of long-term variability. In this model, the 39 *T. occidentalis* residual series were detrended using a spline function giving a 50% oscillation response of 300 years (preserving 99% of the variance contained in oscillations less than 99 years).

2.5 Tree growth and climate relationships

Development of each July CDC sub-reconstruction models was conducted as described by Cook and Kairiukstis (1990), Fritts (1991), and Cook et al. (1994). The

first step involved in the development of the models was to determine which monthly CDC value to reconstruct. Both redundancy analysis (RDA) and principal component analysis (PCA) (Tardif et al. 2003) were used for this purpose. For these analyses, the chronology data set included the 16 site residual chronologies and the climate data set included monthly CDC (from Girardin et al. 2004) and monthly regional temperature and precipitation series (from Tardif and Bergeron 1997b). Both RDA and PCA were performed on correlation matrices and program CANOCO 4.0 was used (Ter Braak and Smilauer 1998).

Redundancy analysis is the canonical extension of PCA and intends to display the main trends in variation of a multidimensional data set in a reduced space of a few linearly independent dimensions (Legendre and Legendre 1998). In RDA, however, the canonical axes differ from the principal components (PCs) in that they are constrained to be linear combination of supplied environmental variables (Ter Braak and Prentice 1988; Ter Braak 1994). RDA may be understood as a two-step process: (1) each site residual chronologies are regressed on the climate variables and the fitted values are computed; (2) a PCA is then carried out on the matrix of fitted values to obtain the eigenvalues and eigenvectors (Legendre and Legendre 1998). The climate variables were selected using a forward selection on the basis of the goodness of fit and tested for significance using a randomization test (9999 Monte Carlo unrestricted permutations). This procedure was repeated until a variable was tested non-significant at the 5% level. RDA was also performed on subsets of site residual chronologies (models II and III) and residual series (models IV and V). For cross verification, a PCA was conducted on the 16 site residual chronologies and the first and second principal components were correlated with the climate variables using the Pearson correlation coefficient.

2.6 July CDC reconstruction

In each July CDC sub-reconstruction model, the site residual chronologies were transformed into orthogonal eigenvectors to remove multicollinearity between the predictors (Cook and Kairiukstis 1990; Legendre and Legendre 1998). In models I, II, and III the 16 residual site chronologies were entered in a PCA and the first and second principal components (which contains over 53% of the total variance) were used in subsequent procedures (Table 1). For models IV and V, the 39 residual measurement series were entered in a PCA. PCI, PCII, PCIII and PCIV (49.5% and 48% of the total variance, respectively for model IV and V) were used later on as July CDC predictors.

Because tree growth in the year of ring formation is influenced by weather conditions in both the current and the prior growing seasons (Cook and Kairiukstis 1990; Archambault and Bergeron 1992; Hofgaard et al. 1999; Fritts 2001), the PCs were forwarded by one year and included in the models. A total of four July CDC predictor time series were included in models I-II and III, and eight in models IV and V.

Calibration models were computed using multiple linear regression analyses between the instrumental drought indices (CDC July monthly averages) and the PCs (present and forward lags) (Cook and Kairiukstis 1990). The yearly July CDC for the early period covered by the site residual chronologies was estimated from the calibration model equations (transfer function). The stability of each model was tested (verification procedure) after conducting two sub-calibrations of the periods 1895–1939 and 1940–1984. Reduction of error (RE), product means test (PM), Spearman rank correlation coefficient and sign test were calculated on the independent periods (period not included in the calibration) according to standard procedures (Cook and Kairiukstis 1990; Fritts 2001).

2.7 Validation with fire history

As a mean of validation, a fire history reconstruction conducted by Bergeron (1991) in the Lake Duparquet area (Fig. 1) was used to validate the ability of the reconstructed July CDC to capture years of severe drought events that often lead to forest fires. This data set consists of years ($\pm$1-year accuracy) of large area burned (>1 km^2) near Lake Duparquet derived from fire-scarred trees. These fire years were 1760, 1797, 1816, 1823, 1847, 1870, 1907, 1919, 1923, and 1944.

2.8 Ocean-atmosphere circulation patterns

One objective of this study is the comparison of the variability in the CDC with that of paleoclimatic indices of atmospheric circulation. Numerous proxy records of interannual and interdecadal scale climate variability for the Pacific and Atlantic sectors exist (Stahle et al. 1998; Cook et al. 1998; Luterbacher et al. 1999; Biondi et al. 2001; D'Arrigo et al. 2001; Glueck and Stockton 2001). Because the reconstructed July CDC is an estimate of spring and early summer climate variability (May–July), paleoclimatic indices spanning this season were prioritized over others for the analysis.

D'Arrigo et al. (2001) presented two annual Pacific Decadal Oscillation (PDO; Mantua et al. 1997) reconstructions, a decadal scale oscillatory mode of North Pacific SST. The two reconstructions (differ in the number of chronologies incorporated in the models) are based on summer temperature sensitive tree-ring chronologies from the Gulf of Alaska and winter sensitive tree-ring chronologies from the southwestern United States (USA) and Mexico. Their 1790–1979 reconstruction accounts for 53% of the instrumental variance while the second reconstruction accounts for 44% of the variance and extends as far back as 1700. The 1790–1979 reconstruction demonstrated better predictive skills, and

therefore it was selected and extended to 1700 by using the segment 1700–1789 from the later reconstruction.

Reconstructed monthly North Atlantic Oscillation (NAO; Rogers 1984; Hurrell 1995, 1996) indices by Luterbacher et al. (1999) were used in this study. Because this data set provides us with the possibility of using NAO seasonal averages of May to July, their record was chosen over Cook et al. (1998) and Glueck and Stockton (2001). The use of a seasonal NAO pattern is particularly appealing since the NAO exerts strong seasonal variations over the Northern Hemisphere (Barnston and Livezey 1987) and at virtually all longitudes (Thompson and Wallace 2001). The NAO can also be viewed as the manifestation of the Arctic Oscillation in the North Atlantic sector (AO; Thompson and Wallace 1998). The NAO reconstruction of Luterbacher et al. (1999) is derived from varying time series of instrumental pressures, temperature, precipitation, and paleoenvironmental records. The period for which excellent results (variance > 30%) were obtained by the authors spans 1770–1990. Prior to 1770, the predictive skills are poor.

Finally, the Southern Oscillation (SO) index (Ropelewski and Jones 1987), an important source of interannual climate variation that influence weather and climate all over the world, was reconstructed by Stahle et al. (1998). Even though the SO reconstruction (which covers the period 1706 to 1977) is restricted to the winter period of December to February, SO anomalies are persistent enough to affect climate many seasons after the onset (Kiladis and Diaz 1989; Bonsal and Lawford 1999).

2.9 Spatiotemporal analyses

Common variance at multiple-scales between the July CDC reconstruction and the reconstructed atmospheric circulation pattern indices (NAO, PDO, and SO) was analyzed using PCA conducted on correlation matrices. Five 100-year intervals, held in common by all reconstructed variables, from 1706 to 1979 were used (note that the period chosen was constrained by the length of the SO reconstruction). The first PCA was conducted on the period 1706–1805 whereas the last one was conducted on the period 1880–1979. A PCA was also conducted on instrumental circulation pattern indices (monthly average of May to July) for the period 1900–1998. For this analysis uniquely, instrumental AO indices as well as reconstructed CDC indices were added as supplementary (passive) variables. Passive variables do not influence the formation of the PCs. They are added afterwards in the analysis so that their relation to the other variables can still be judged from the reduced space (representation of a large fraction of the variability of a multidimensional data matrix, in a space with reduced (i.e. lower) dimensionality relative to the original data set (Legendre and Legendre 1998)).

2.10 Spectral analyses

Fourier multitaper spectra analyses (Lees and Park 1995; program AutoSignal version 1.5; AISN Software 1999) were conducted on the reconstructed July CDC for identification of stationary signals. Analyses of peak-based critical limit significance levels were performed for ascertaining the significance of the largest spectral component. In this type of test, one seeks to disprove the null hypothesis where one postulates either a white noise signal (AR(1) = 0.0), or a red noise signal (AR(1) > 0.0) (Lees and Park 1995). Red noise is present when the background power decreases with increasing frequency.

In the Fourier method, the component sine and cosine waves are localized in frequency but not in time (Torrence and Compo 1998). This is problematic when analyzing time series with non-stationary signals. Alternatively, continuous wavelet transform (CWT) analyses were used to decompose signals into wavelets, small oscillations that are highly localized in time (Torrence and Compo 1998). Whereas the Fourier transform decomposes a signal into infinite length sines and cosines, effectively losing all time-localization information, the CWT's basis functions are scaled and shifted versions of the time-localized mother wavelet. The CWT is used to construct a time-frequency representation (spectrum) of a signal that offers very good time and frequency localization. Coherency between two time series (CDC against the NAO, the PDO, and the SO) at various time and period scales were identified by the cross products of the CWTs from the two time series (Torrence and Compo 1998; Torrence and Webster 1999). Periodicities showing coherency were reconstructed with the use of spectral components isolated in the time-frequency domain (wavelet filtering and reconstruction; Torrence and Compo 1998).

In this study, CWT analyses were performed using a nonorthogonal Morlet wavelet basis (wave number of 6), a Gaussian-windowed complex sinusoid (Torrence and Compo 1998). The wavelet basis was selected so that the time-space domain is maximized in length over the spectral-space domain (Torrence and Compo 1998). Other wavelet basis procedures (the Paul basis for instance) with various adjustable parameters were also tested and results tended to be consistent (within the uncertainty of the wavelet basis' definition). For the spectrum analyses, all reconstructions were updated to 1998 by using instrumental meteorological data (calculated as per the original method). Also, the SO data set (1706–1977) was padded with additional zeros for the years 1700–1705 for consistency with the PDO data set length. All reconstructed indices (CDC, NAO, PDO, and SO) were normalized before processing the CWT. CWT analyses were performed using the program AutoSignal version 1.5 (AISN Software 1999) and using IDL (Interactive Data Language, Research Systems) wavelet programs written by Torrence and Compo (1998).

2.11 Geopotential height maps

For validation of the relationship between the CDC and atmospheric circulation during the instrumental climate period, May-July 500-hPa geopotential height composite and correlation maps were created with the aid of the NOAA-CIRES Climate Diagnostics Center, Boulder Colorado (Kalnay et al. 1996; www.cdc.noaa.gov). The 500-hPa grid has a global spatial coverage of 2.5° latitude by 2.5° longitude with 144 × 73 points and a temporal coverage of 1948 to present, with output every 6 hours. Daily 500-hPa heights (expressed in m) were averaged by months for each grid point. For the composite maps, 500-hPa anomalies were determined relative to the mean value of the 1968–1996 reference period.

3 Results

The climate variable showing the strongest relationship with the sixteen site residual chronologies was the July monthly average CDC (Fig. 2, Table 2). Both RDA canonical axes were well correlated with this variable (Fig. 2). Temperature and June precipitation also accounted for an important part of the variability, particularly the temperatures prevailing in August the year prior to ring formation and in early spring of the year of ring formation (Fig. 2). With respect to seasonal variables, the correlation coefficients obtained from the July CDC indices exceeded those obtained from seasonal average temperature and total precipitation (Table 2). Correlation analyses (Table 1) indicated that the most drought sensitive site residual chronologies were *B. papyrifera*, and *P. banksiana* of Lake Hébécourt and Lake Duparquet. Chronologies of *T. occidentalis* from dry sites of Lake Duparquet, and of *P. mariana* from Hedge Hills and Lake Hébécourt also correlated well with the July CDC (Table 1). Redundancy analysis conducted on subsets of site residual chronologies (models II and III) and on *T. occidentalis* residual series (models IV and V) also identified the July CDC value as a significant climate variable (results not shown).

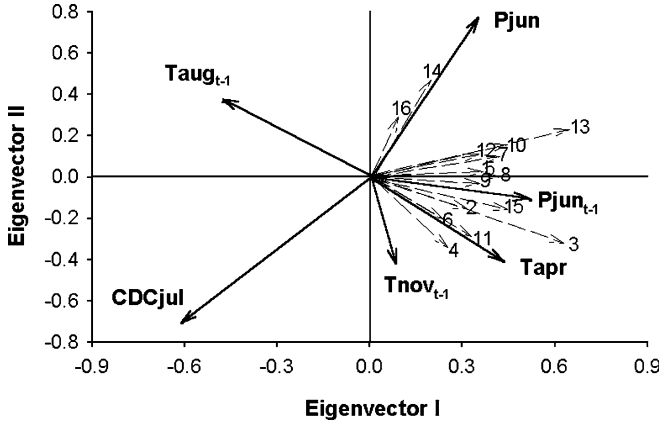

Fig. 2 Eigenvectors of the redundancy analysis (RDA) conducted on the site residual chronologies from the Abitibi Plains ecoregion. The descriptors (*arrows*) are positioned in the biplot based on their correlations with the canonical axes. For instance, the variable *CDCjul* has a correlation of –0.61 with the first canonical axis and of –0.71 with the second one. In addition, the biplot also approximates the correlation coefficient among descriptors and climatic variables (Legendre and Legendre 1998). Climate variables and site residual chronologies with *arrows at sharp angles* are positively correlated (cos 0° = 1.0, i.e. perfect correlation). Conversely, obtuse angles indicate negative correlation (cos 180° = –1.0, i.e. perfect correlation). Variable abbreviations are June precipitation ($Pjun_{t-1}$) and November ($Tnov_{t-1}$) and August ($Taug_{t-1}$) temperatures of the year prior to ring formation, and June precipitation (*Pjun*), April temperature (*Tapr*) and July drought (*CDCjul*) of the year of ring formation. Refer numbers to Table 1 for identification of site residual chronologies. Eigenvalues (*E*) and descriptors - climate correlation coefficients are $E_1 = 0.129$, $E_2 = 0.075$, $r_1 = 0.598$, and $r_2 = 0.655$; percentage of explained variance of descriptors - climate relation are canonical axis I = 0.54 and canonical axis II = 0.31. The significance of all canonical axes is $P < 0.001$

3.1 Reconstructed July CDC

Correlation analyses and visual assessment indicated that the interannual and interdecadal variability contained in the instrumental July CDC value was adequately reproduced in model I ($P < 0.001$; Fig. 3a). The Spearman rank correlation, sign tests, reduction of

Table 2 Pearson correlation coefficients between monthly average CDC indices and PCI and PCII of the sixteen site residual chronologies

	PCI	PCII
Monthly average CDC		
Year prior to ring formation		
April	–0.04	–0.05
May	–0.02	0.04
June	–0.16	0.05
July	–0.20	0.24
August	–0.18	0.12
September	–0.09	0.07
October	–0.03	0.00
Year of ring formation		
April	0.21	–0.20
May	0.08	–0.18
June	–0.17	–0.28
July	–0.36	–0.42
August	–0.15	–0.35
September	–0.05	–0.23
October	–0.10	–0.05
May–July average temperature		
Year prior to ring formation	0.14	–0.05
Year of ring formation	–0.18	–0.31
May–July total precipitation		
Year prior to ring formation	0.22	–0.15
Year of ring formation	0.25	0.42

Correlation coefficients conducted on May to July average temperature and total precipitation are also shown. Coefficients are significant at $P < 0.05$ when $r > |0.21|$. The two PCs accounted for 52.6% of the total variance

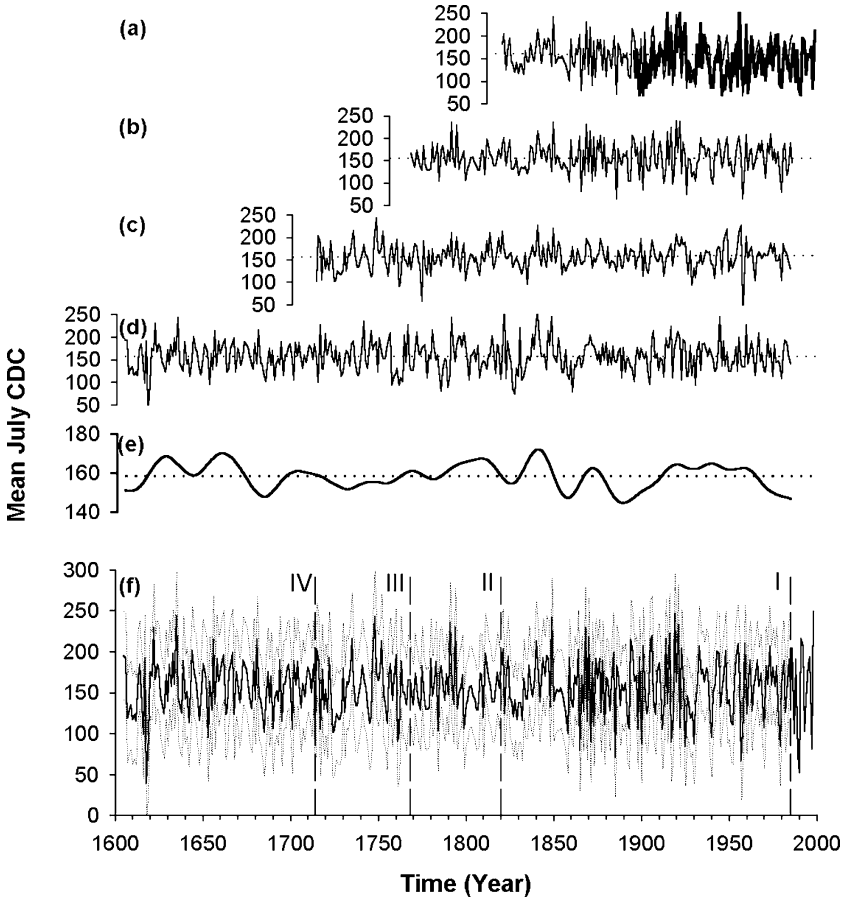

Fig. 3a–e Sub-reconstructed July CDC models I to V. A Savitzky-Golay Smoothing Filter procedure was performed on the fifth model **e**. This time-domain method of smoothing is based on second degree least squares polynomial fitting across a moving window within the data. **f** Final July-CDC reconstruction made from segments (delineated by *dashed lines*) of models I, II, III and IV and updated using instrumental CDC indices (period 1985–1998). Error bars are shown in **f** by *thin dotted lines*. In **a** is also shown the instrumental CDC indices (*thick line*)

error (RE), and product means test (PM) statistics of the verification (Table 3) supported this statement by indicating significant predictive skills of the calibration model (Cook and Kairiukstis 1990; Cook et al. 1994; Fritts 2001). Whenever RE is greater than zero the reconstruction is considered as being better than the calibration period mean, indicating a tendency for the reconstruction to reproduce with confidence both high- and relatively low-frequency drought variations. A significant sign test indicates good fidelity in the direction of year-to-year drought change in the real and estimated data, while the PM test result indicates that the magnitudes as well as the direction of these changes are statistically significant. Based on results of Table 3, we considered the reconstruction to be reliable from 1768 to present as an estimate of interannual and interdecadal climate variability. Prior to 1768, partially positive RE statistics indicated that the regression models on the average had some skill and that the reconstructions were of some value. A partitioning (Cook and Kairiukstis 1990) of the negative RE value from models III and IV indicated that the RE were effectively greater than the RISK factor (–0.63 and –0.44, respectively). It is recognized that values of RE that are negative but greater than the measure of the variability of both estimates and instrumental observation (RISK) may still contain some meaningful climate information. Loss in variability is however observed from model I to model IV (Fig. 3a–3d, respectively) judging by the intermodel Spearman rank correlation coefficients (r) (period 1895–1984: $r_{\text{I-II}} = 0.98$, $r_{\text{I-III}} = 0.63$, and $r_{\text{I-IV}} = 0.55$). As for model V (Fig. 3e) in which intercentennial variability was preserved, statistics ($r^2 = 0.46$; RE = 0.08 and –0.14) were very similar to model IV (Fig. 3d; Table 3).

During the time span of the reconstruction, 32 years of high drought indices (above 200 as suggested by Turner 1972) were estimated between 1605 and 1984 (Fig. 3f, Appendix 2). Eleven of these years occurred during the early twentieth century at time when interannual variability was the greatest (Fig. 3f). Reconstruction of intercentennial variability showed that long-dry periods occurred during the late eighteenth and the nineteenth century: 1760s, 1790s–1810s, 1830s–1840s, and 1860s–1870s (Fig. 3e). Very dry climate was also observed in the seventeenth century, with in addition strong interdecadal signals.

A multitaper spectra analysis of the reconstructed July CDC 1700–1998 period showed no significant stationary signals (Fig. 4a). Analyses of two independent periods, pre-1850 and post-1850, however indicated that signals at around 14–36 year/cycle, although not significant, were considerably more pronounced during the interval 1700–1849 relative to 1850–1998 (Fig. 4b, 4c). These signals contributed to the small

Table 3 Calibration and verification statistics of all four sub-reconstruction models (Cook and Kairiukstis 1990; Fritts 2001)

	MODEL I (1820)			MODEL II (1768)		
Calibration periods	1895–1939	1940–1984	1895–1984	1895–1939	1940–1984	1895–1984
Verification periods	1940–1984	1895–1939	–	1940–1984	1895–1939	–
Calibrations						
Multiple *r*	0.69	0.58	0.63	0.70	0.52	0.61
r-square	0.48	0.34	0.40	0.49	0.27	0.38
Adjusted *r*-square	0.43	0.27	0.37	0.44	0.20	0.35
Standard error of the estimate	48.52	49.20	48.46	48.04	51.55	49.23
Analyses of variance						
P-value	0.000	0.002	0.000	0.000	0.011	0.000
Verifications						
Reduction of error [c]	0.29	0.47	–	0.23	0.41	–
Product means test [d]	2.67	3.62	–	2.66	3.62	–
Spearman rank correlation	0.51	0.65	0.60[b]	0.47	0.64	0.58[b]
Sign tests[e]						
Agreements	33	33	–	30	30	–
Disagreements	12	11	–	15	15	–
P-value	0.005	0.005	–	0.050	0.050	–
	MODEL III (1714)			MODEL IV (1605)		
Calibration periods	1895–1939	1940–1984	1895–1984	1895–1939	1940–1984	1895–1984
Verification periods	1940–1984	1895–1939	–	1940–1984	1895–1939	–
Calibrations						
Multiple *r*	0.54	0.45	0.43	0.52	0.67	0.54
r-square	0.29	0.21	0.18	0.27	0.45	0.29
Adjusted *r*-square	0.22	0.13	0.15	0.11	0.33	0.22
Standard error of the estimate	56.56	53.77	56.12	60.45	47.22	53.90
Analyses of variance						
p-value	0.007	0.052	0.002	0.148	0.003	0.000
Verifications						
Reduction of error[c]	–0.21	0.02	–	0.20	–0.05	–
Product Means test[d]	[a]	[a]	–	2.79	[a]	–
Spearman rank correlation	0.32	0.27	0.43[b]	0.41	0.27	0.52
Sign tests[e]						
Agreements	25	29	–	31	27	–
Disagreements	20	16	–	14	18	–
P-value	[b]	[b]	–	0.020	[b]	–

[a]Non-significant
[b]Correlations between estimated and instrumental data ($P < 0.001$ if $r > 0.35$)
[c]Positive values signify predictive skills
[d]Significant tests indicate that large departures from the mean are reconstructed any more reliably than smaller ones
[e]Agreements indicate correct sign of tree-ring estimates

amount of red noise observed in the spectra (AR(1) > 0; refer to Sect. 2.10). Interannual signals (2.05–2.69 and 3.58–3.77 year/cycle) were considerably more pronounced after 1850.

3.2 Validation with fire history

To validate the ability of the final CDC reconstruction to estimate past seasons of drought, yearly historical records of extensive burned area were compared with the reconstruction. Observation showed concordance between large areas burned in the vicinity of Lake Duparquet and years of drought. Out of the ten fires reported, six (1760, 1847, 1870, 1919, 1923, and 1944) accurately corresponded to drought estimates higher than 190 (Appendix 2). Fires in 1823 and 1907 corresponded with dry years estimated in 1822 and 1906, respectively. Fires in 1797 and 1816 did not corresponded to severe drought indices.

3.3 PCA and atmospheric circulation

PCA was used to investigate the common variability structure between the reconstructed July CDC and patterns of atmospheric circulation (PDO, SO and NAO). As a result of the varying site chronologies in the climate reconstruction process, caution must be taken when interpreting the correlations with atmospheric circulation patterns before 1770.

Reduced spaces in Fig. 5 all demonstrated that PCI was negatively correlated with the PDO and positively with the SO. The angle approximating 180° between the two vectors further highlighted the negative correlation between the two circulation patterns. As for PCII, it was

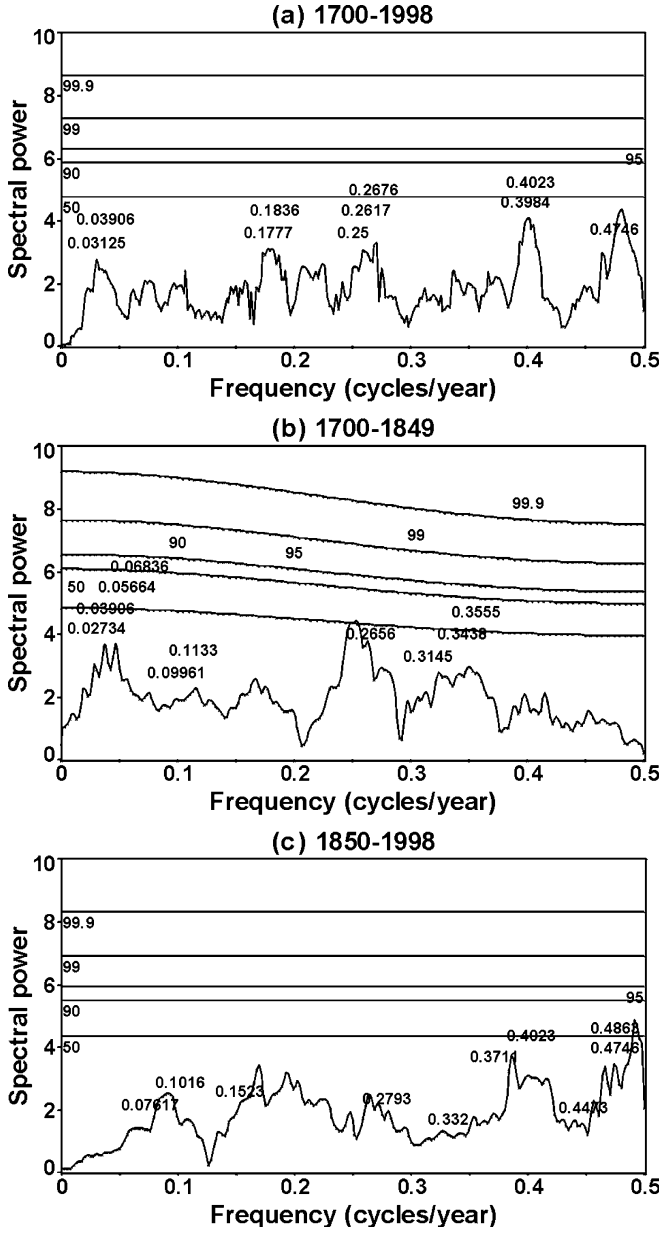

Fig. 4 Fourier multitaper spectra of the CDC reconstruction for **a** 1700–1998, **b** 1700–1849, and **c** 1850–1998. The 50, 90, 95, 99, 99.9% significance levels are indicated (lag-1 autoregressive spectrum AR(1) = 0.00 in **a** and **c**, and = 0.05 in **b**. The frequency locations of the detected peaks were drawn from the F-ratio maxima, and only those with F-ratio values exceeding 2.0 were processed as spectral peaks (*displayed on plots*). Target peaks to detect was set at 10. For each peak, the period (years/cycle) is given by the conversion 1/frequency

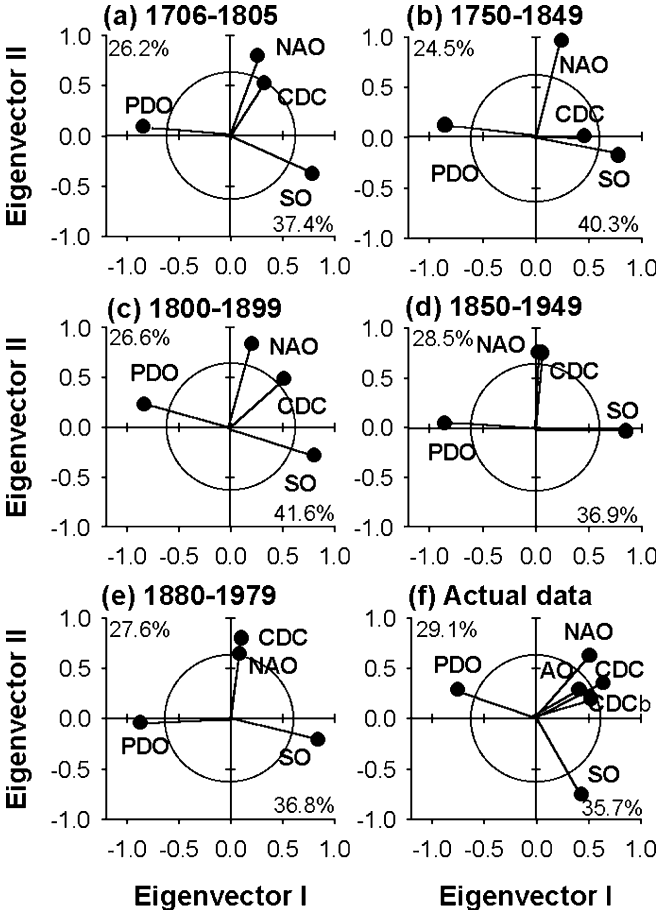

Fig. 5a–e Eigenvectors of the principal component analyses (PCA) illustrating the relationships among the reconstructed July CDC, the NAO, the PDO, and the SO through time. Five 100-year intervals **a–e** are shown and each demonstrates the correlation coefficient between the reconstructions and PCI and PCII (the descriptors are positioned based on their correlations with the PCs). The correlation among descriptors is also approximated and those with *arrows at sharp or obtuse angles* are positively or negatively correlated, respectively (either cos 0° = 1.0 or cos 180° = –1.0, i.e. perfect correlation). The *circle of equilibrium* enables us to judge whether the contribution of each index to the reduced space is greater or smaller than expected under the hypothesis of an equal contribution to all principal components (Legendre and Legendre 1998). Indices that are clearly shorter than the value of their respective equilibrium contributions contribute little to the formation of the reduced space. A sixth plot **f** shows results of a PCA conducted on instrumental circulation pattern and drought indices for the period 1900–1998. For this last analysis, the AO index as well as the reconstructed CDC (CDCb) were added as supplementary descriptors for comparison with their analogue. *Percentages of variance* captured by PCI and PCII in the principal component analyses are also shown

positively and highly correlated with the NAO. Angles approximating 90° between the NAO and the SO and PDO suggested the absence of a correlation between the North Atlantic and the Pacific sectors. In every reduced space, the contribution of the NAO, PDO, and SO to the formation of PCI and PCII exceeded the expected one under the hypothesis of an equal contribution to all principal components (by comparing the length of the descriptors' projection to the equilibrium circle). Percentages of explained variance by PCI and PCII remained relatively constant from one period of analysis to another (Fig. 5).

Reduced spaces demonstrated a positive correlation between the CDC and the NAO (sharp angle) along PCII at the beginning and end of the period of analysis (Fig. 5a, d, e). No correlation with the SO and PDO

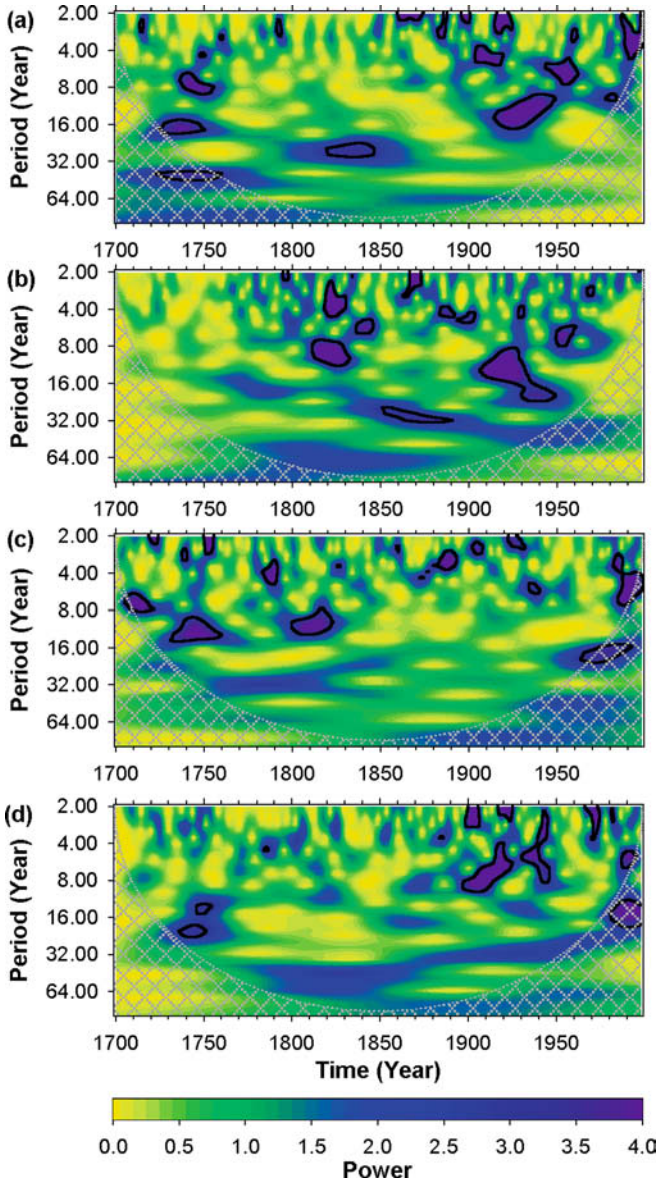

Fig. 6a The CDC, **b**the NAO, **c** the PDO and **d** the SO continuous wavelet transformation (CWT) power spectrums. The wavelet power at each period is normalized by the global wavelet spectra (GWS; Torrence and Webster 1999). The *dark blue color* indicates areas of large power equal three times the GWS. *Black contour* is the 5% significance level above the GWS. The *crosshatched regions* on either end indicate the cone of influence (edge effect; Torrence and Compo 1998; Zheng et al. 2000), where zero padding has reduced the variance

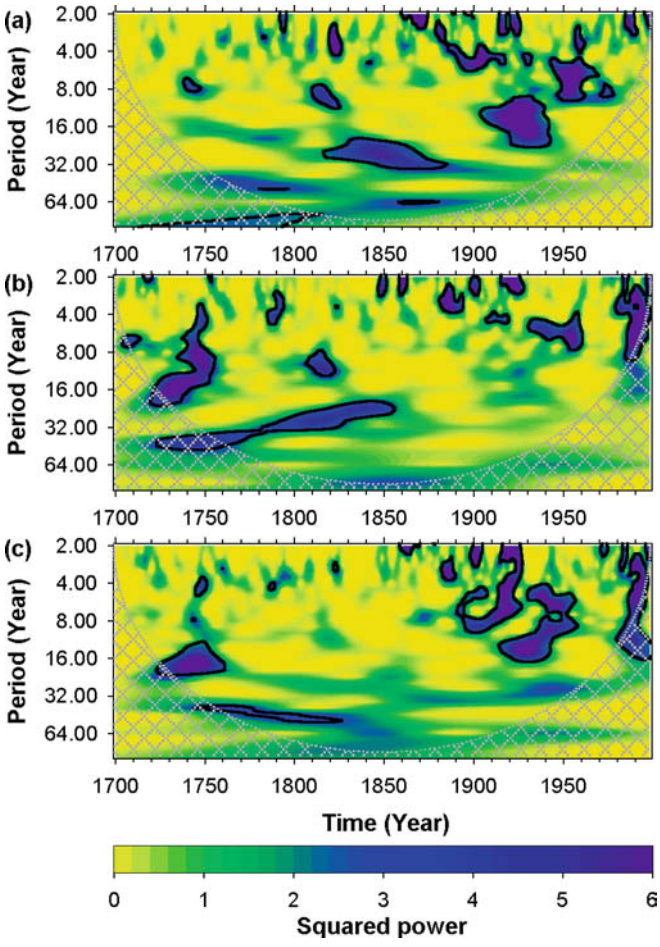

Fig. 7 Cross-CWT power spectrums of **a** the CDC and the NAO, **b** the CDC and the PDO, and **c** the CDC and the SO. The *dark blue color* indicates coherency in time and period scales. *Black contour* is the 1% significance level. The *crosshatched regions* on either end indicate the cone of influence, where zero padding has reduced the variance

(angles close to 90°) was observed. This configuration shifted in the middle of the eighteenth century (1750–1849) as the correlation between the NAO and the CDC decreased (Fig. 5b,c), suggesting that the CDC may have been subject to another external forcing. The position of the CDC vector in relation to those of the PDO and SO suggested that the 1750–1849 forcing could have originated from the Pacific sector. Analysis conducted on instrumental circulation pattern and CDC indices indicated a correlation structure similar to the one observed using paleoclimatic indices (Fig. 5f). Also, the analysis indicated that variability in the CDC was better explained by the use of the NAO index rather than the AO index.

3.4 CWT and atmospheric circulation

The coherencies between the CDC reconstruction and the NAO, the PDO, and the SO reconstructions were evaluated using CWT analyses (Figs. 6, 7, and 8). As the Fourier multitaper spectra analyses highlighted the problematic of non-stationary signals in the CDC reconstruction (Fig. 4), CWT analysis was performed on each individual series for mean of comparison of the stationary sections. The analyses (Fig. 6a) indicated that strong 17–32-years oscillations in the CDC characterized the eighteenth and the nineteenth centuries. Similar analyses performed on the PDO, NAO and SO reconstructions revealed that the PDO (Fig. 6c) also

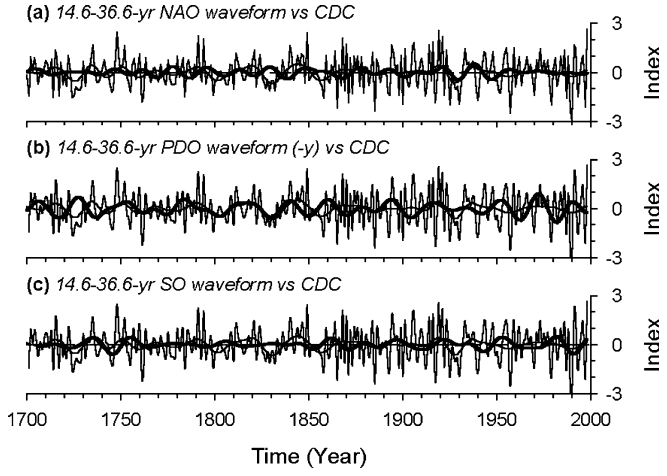

Fig. 8 The 14.6–36.6-year/cycle wave forms of the **a** NAO, **b** PDO and **c** SO (*all thick lines*). The normalized CDC (*thin line*) as well as its 14.6–36.6-year/cycle wave form (*thin smooth line*) are also shown. Signs of the PDO were inverted (-*y*) for a better fit

showed high power in that range of frequencies from the middle eighteenth century to early nineteenth century. The NAO demonstrated a similar signal, but post the 1840 (Fig. 6b). The coherency between the PDO and the CDC prior to 1850 was further highlighted by the cross-CWT analyses (Fig. 7b) and the reconstructed spectral components isolated in the time-frequency domain (Fig. 8b). It was found that the Spearman correlation between the CDC reconstruction and the PDO 17–32-year wave form was 14.2% ($P < 0.001$) for the period 1760–1840. The correlation increased to 54.8% when the PDO and CDC wave forms were correlated together. For the period post 1850, the CDC synchronized intermittently with the NAO wave form, with maximum synchronization occurring in the first half of the twentieth century (Fig. 7a). The two wave forms (CDC versus. NAO, Fig. 8a) shared 36.2% ($p < 0.001$) of common variance during the period 1880–1940. Prior to 1750, some coherency with the SO was observed (Figs. 7c, 8c).

Coherency between the PDO and the CDC prior 1850 was further highlighted in the 9–16-year oscillation band (Fig. 7b). Additionally, some coherency with the SO was observed around 1750 (Fig. 7c) and with the NAO and SO in the first half of the twentieth century (Fig. 7a,c). At last, dispersed 2–8-year oscillations in the CDC (Fig. 6a), though more prominent in the last century, were shown to be coherent with all three patterns (Fig. 7). However, greater coherency with the SO was observed from 1850 to 1950, and more specifically from the 1910s to the 1940s (Fig. 7c). Observed coherency in the late twentieth century may be affected by the edge effect (results from a discontinuity at the end of the data stream). Cross-CWT analyses conducted on instrumental pattern indices and instrumental CDC indices (analyses not shown) show patterns of coherency similar to that observed using reconstructed indices.

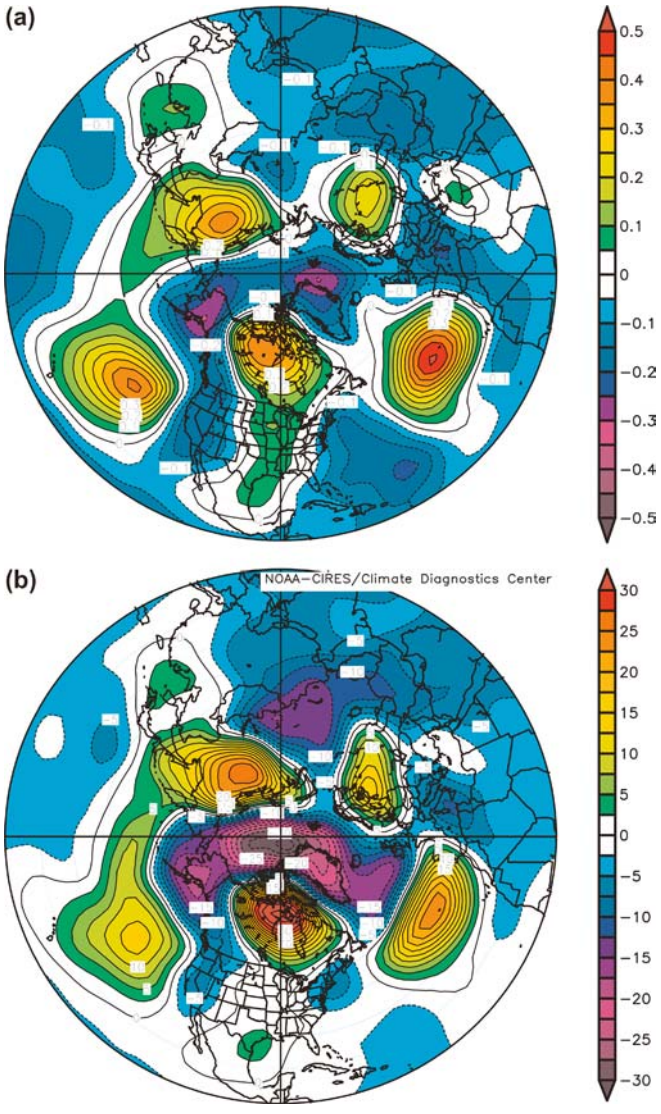

Fig. 9 The 500-hPa geopotential height **a** correlation and **b** composite maps (period 1948–1998). The May to July season was used in the calculation of the height data (in m). In **a**, correlation coefficients are significant at $P < 0.05$ when $r > |0.27|$. In **b**, the anomalies were calculated by subtracting the height anomaly values from the ten driest years minus the ten years of lowest drought severity

3.5 The 500-hPa geopotential height maps

Sections 3.3 and 3.4 suggested that July drought during the instrumental period was mainly driven by the North-Atlantic circulation mode. This is confirmed for the later part of the twentieth century with the creation of the 500-hPa composite and correlation maps (Fig. 9). The dipolar pattern that characterizes the NAO (inverse anomalies above Iceland and the Azores) was well reproduced, particularly in the composite map. In association with severe drought seasons, both maps were coherent by showing anomalous ridging (centered above Baffin Bay) over the Abitibi Plains. The ridge was accompanied by a northward deflection of the moisture

carrying system. During low drought seasons, the ridge was displaced northeastward allowing the moisture carrying system to penetrate above the area of study. In addition to the North Atlantic circulation mode, a center of positive correlation was observed in the North Pacific.

4 Discussion

4.1 July CDC reconstruction

In the Abitibi Plains ecoregion the results show that drought is among the most significant variable affecting ring-width when all site residual chronologies are combined. However, because the July CDC reconstruction was developed from varying site residual chronologies, the climate variability captured by the PCs is lacking in stability with removal of site residual chronologies. While the drought signal captured by model I was perfectly reproduced in model II after the removal of eight site residual chronologies, removal of three additional chronologies prior 1768 (model III) contributed to a substantial decrease in the confidence of the sub-reconstruction models. Visual assessment and additional CWT analyses (not presented) conducted on sub-reconstruction models however demonstrated that non-stationary signals prior 1850 on which this work focuses are well reproduced from one model to the other.

The multitaper spectra and CWT analyses of drought variability in the Abitibi Plains ecoregion highlighted a shift in time scale variability from an interdecadal toward a more pronounced interannual forcing. In addition, while the 'Little Ice Age's climate was characterized by dryer decades (as revealed by the CDC-low frequency reconstruction, model V), the early twentieth century was an unprecedented period characterized by a high frequency of severe drought seasons. Interestingly, the largest forest fires of the last 150 years in eastern Canada were encountered during the 1910s and 1920s (Bergeron et al. 2001). Prior to 1850, large forest fires occurred during the 1760s–80s and the 1810s–1840s (Bergeron et al. 2001).

4.2 Atmospheric circulation patterns

Analyses linking drought variability to major features of Northern Hemisphere circulation have identified a changing relationship over the past 300 years. This is such that if a 500-hPa geopotential height scenario had to be drawn for the period 1750–1850, it would be unlikely to be similar to the 1948–1998 configuration (Fig. 9). Our results lead us to suggest that the end of 'Little Ice Age' ($\backsim$1850–1870) over the Abitibi Plains sector corresponded to a decrease in the North Pacific decadal forcing around the 1850s. This event could have been followed by an inhibition of the Arctic air outflow and an incursion of more humid air masses from the subtropical Atlantic climate sectors.

The mechanisms linking warm season regional climate variability with ocean-atmospheric circulation patterns are not firmly established. For that reason it is difficult to provide a precise explanation of the cause of the 1850s atmospheric circulation shift over the Abitibi Plains ecoregion. However, description of the PDO/SO winter modulations by Bonsal et al. (2001; investigation based on analyses of the instrumental data) may provide some insights. Bonsal et al. (2001) showed that in the winter season, a +PDO/–SO phase is associated with a deeper than normal Aleutian low, an amplification and eastward displacement of the western Canadian ridge, and negative height anomalies over the southeastern USA. This combination reflects a northward-displaced polar jet stream, which inhibits the outflow of Arctic air over most of Canada. The reverse is true for the –PDO/+SO phase but with weaker effects. The evidence of a -PDO phase (warmer water in the interior Pacific and cooler water along the North Pacific coast; Mantua et al. 1997) from approximately 1750–1850 has been demonstrated with the investigation of prominent aquatic population declines in the Gulf of Alaska (Finney et al. 2000). A North Pacific forcing from 1750–1850 may thus have resulted in a modification of the circulation flow over the Abitibi Plains ecoregion.

There are several types of evidence suggesting the implication of ocean-atmospheric circulation patterns anomalies in extreme climate conditions of the last century. Nigam et al. (1999) and Barlow et al. (2001) demonstrated that Pacific decadal SST variability was strongly linked to large-scale patterns of warm-season drought and stream flow in the USA. Bonsal et al. (1993) and Bonsal and Lawford (1999) reported similar findings after documenting and analyzing teleconnections between the SO, North Pacific SST, and summer extended dry spells over the Canadian Prairies. Nigam et al. (1999) also hypothesized that SST anomalies in the North Atlantic Ocean, by creating positive feedback with circulation anomalies from the Pacific, could contribute to enhanced drought seasons in the northeast USA. Moreover, implication of North Pacific SST in the regulation of Canadian boreal forest climatically induced disturbances as been postulated. Skinner et al. (1999) demonstrated a linkage between wildland areas burned and the presence of anomalous ridging at 500-hPa immediately over western and west-central Canada. In another study, Flannigan and Wotton (2001) demonstrated a linkage between Pacific SST and seasonal forest area burned in eastern Ontario. While ocean-atmosphere circulation patterns are reported to be mostly effective during winter, this study and those enumerated suggests that their regional impacts during the summer period could be underestimated.

Concerns are presently being directed toward recent changes in the North Pacific where a reversal of the PDO in the 1940s toward more pronounced decadal variability is suspected to be occurring (Hare and Mantua 2000; D'Arrigo et al. 2001). In our study, recent decadal signals (period post-1946) associated with the

PDO were not clearly apparent. Preliminary analyses in the central Canadian boreal forest (western Manitoba), however, tend to suggest that climate in central Canada may be responding to a reversal of the circulation pattern (Girardin et al. 2002b, 2004). Strong decadal signals starting in the 1940s and coherent with the PDO are dominating the central Canada CDC spectra. As information gained from a dendroclimatological study conducted along a southern Canadian boreal forest transect will provide some insight on the speculated displacement of the jet stream around 1850, forecasting of future changes will require more extensive study. There is a need to develop an extensive network of dendrochronological data and climate reconstructions in Canada. This would enable the identification of sensitive regions. A network could also provide an additional time window for simulations of climate with general circulation models (Bradley 1999; Flannigan et al. 2001) and regional circulation models (Laprise et al. 2003). Further analyses will help forecasting the potential effect of anthropogenic climatic change, which could alter variations in low-frequency oscillations.

Our comprehension of the impacts of climate dynamics is not complete without considering the relationship between ocean-atmosphere circulation shifts and population dynamics over multicentury intervals (Finney et al. 2000; D'Arrigo et al. 2002). Biological processes might be more closely tied to atmospheric circulation than expected and this may affect projections of future changes in population dynamics (biodiversity, richness, and abundance). Natural resources management (water, fisheries, agriculture, forestry, and fauna) could greatly benefit from such understanding.

Acknowledgements We thank S. Archambault, F. Biondi, D. Charron, E.R. Cook, R. D'Arrigo, M.F. Glueck, A. Hofgaard, R. Holmes, B. Lewis, J. Luterbacher, N. Mantua, D.W. Stahle, the International Tree-Ring Data Bank, and the National Oceanic & Atmospheric Administration who contributed to this research by providing us with their data and/or software. CWT and cross-CWT power spectrum analyses were performed using the wavelet software provided by C. Torrence and G. Compo. We also thank B.M. Wotton for his guidance throughout the computation of the daily Canadian Drought Code. This manuscript was improved through the comments of W. Lawrence Gates (editor), M. Cleaveland, three anonymous reviewers, and B. Laishley. Finally we acknowledge the Sustainable Forest Management Network of the Centre of Excellence for providing the funding for this research. During this study, M.P. Girardin received scholarships from the Fonds québécois de la recherche sur la nature et les technologies (FQRNT) and the Groupe de recherche en écologie forestière inter universitaire (GREFi).

Appendix 1

The CDC computation procedure has been reviewed by Girardin et al. (2004). Only the basis is described in this section.

First, simulation of snowmelt is performed (refer to Girardin et al. 2004). At that time (day_d), one proceeds with computation of the CDC by attributing a starting value of 15 to current drought (D):

$$\mathrm{CDC} = D + 0.5\mathrm{PET} \tag{1}$$

The calculation of the potential evapotranspiration (PET; from Thornthwaite and Mather 1955) is given by:

$$\mathrm{PET} = 0.36T + L \tag{2}$$

T represents the maximum daily value of temperature at day_d and Lrepresents a seasonal daylength adjustment. From months of April to October, the values of L are 0.9, 3.8, 5.8, 6.4, 5.0, 2.4, and 0.4 (Van Wagner 1987).

The computation is carried to day_{d+1} with the computation of the rainfall phase (RP):

$$\mathrm{RP} = [800/\exp(\mathrm{CDC}_{d-1}/400)] + 3.937\mathrm{ER} \tag{3}$$

The RP represents the moisture equivalent after rain and is expressed in % of dry soil. The RP scales from 0 to 800, 800 being saturation in water and 0 the driest condition normally encountered. The RP never exceeds 800; excess water is considered as runoff and not accounted for by the CDC. CDC_{d-1} represents the drought value of the previous day and ER (effective rainfall; represents the amount of rainfall available for storage after interception by the canopy) is calculated from:

$$\mathrm{ER} = 0.83P - 1.27 \tag{4}$$

where P represents the daily value of precipitation for day_{d+1} above 2.80 mm (intercepted rainfall). The ER is not computed unless precipitation exceeds that amount of precipitation.

Current drought (D) for day_{d+1} is computed using:

$$D = 400\ln(800/\mathrm{RP}) \tag{5}$$

where the constant 400 represents the maximum theoretical moisture content of the soil. Using Eqs. (5) and (2), one proceeds with the computation of the CDC (Eq. (1)) for day_{d+1}. The procedure is carried over until October 31st.

Appendix 2

Table 4 Annual values of the July CDC reconstruction (1605–1998). CDC values above or equal to 200 are in bold

1605						195.6	193.2	119.2	130.1	135.5
1610	117.5	123.8	115.9	170.6	185.1	153.4	99.4	192.0	40.4	97.9
1620	176.0	170.6	**230.0**	166.7	185.0	177.4	148.1	134.3	124.2	172.0
1630	139.9	184.4	157.9	198.1	160.4	**244.1**	144.9	133.5	125.8	189.7
1640	142.0	151.7	114.1	152.1	**201.7**	173.8	167.5	139.0	116.3	141.7
1650	185.4	177.4	168.0	95.5	163.9	128.8	**215.1**	136.0	191.9	163.8
1660	174.9	190.2	196.2	123.6	133.7	175.6	188.6	198.9	123.3	175.5
1670	162.5	137.7	158.9	190.0	182.9	178.1	160.8	139.5	130.6	187.1
1680	141.4	**215.2**	145.4	141.9	121.8	101.9	138.7	176.1	138.4	170.5
1690	106.4	143.7	152.3	139.7	190.3	115.7	160.4	160.1	180.6	185.0
1700	150.6	105.2	189.2	159.7	188.2	161.4	131.3	161.3	145.3	165.7
1710	181.3	172.2	150.8	184.6	101.7	**203.7**	187.8	105.5	178.3	130.3
1720	154.0	126.3	192.5	159.0	101.8	105.9	125.0	120.3	117.4	128.4
1730	179.9	126.2	163.4	160.2	181.6	**216.0**	163.2	134.3	134.2	148.3
1740	164.2	183.8	163.5	156.4	136.5	112.7	121.9	192.8	**243.4**	174.8
1750	165.3	177.3	**213.8**	147.4	138.4	113.0	171.1	186.0	140.7	169.0
1760	196.3	91.3	104.2	188.4	150.6	150.7	135.3	165.6	166.2	148.6
1770	135.6	173.6	156.2	140.0	129.0	182.7	143.9	129.6	129.7	132.9
1780	191.9	146.3	165.2	188.7	103.5	173.3	182.7	155.3	141.1	173.2
1790	148.2	**236.0**	157.9	136.2	**229.5**	130.6	150.0	157.4	171.8	106.6
1800	136.0	141.4	157.3	158.3	147.3	142.5	129.1	130.4	174.0	171.9
1810	119.9	197.9	184.3	164.5	158.8	138.7	139.8	156.5	174.5	155.9
1820	182.2	**203.9**	124.7	166.5	195.1	145.6	137.9	120.7	141.2	117.3
1830	137.7	137.9	116.2	167.7	142.8	142.4	183.4	155.8	144.9	168.9
1840	**213.8**	186.5	138.9	165.8	192.6	170.2	195.5	190.7	133.0	**242.2**
1850	139.9	148.5	154.2	151.9	155.8	147.7	135.8	125.2	100.2	192.8
1860	142.8	132.4	171.5	159.3	**202.5**	79.5	171.5	127.6	**230.1**	115.9
1870	**218.3**	90.3	187.8	109.3	192.2	167.4	192.2	125.9	189.6	111.0
1880	168.8	165.4	128.2	164.1	199.1	71.7	184.2	168.1	134.4	160.6
1890	152.3	162.4	113.3	106.7	**215.4**	198.7	163.9	171.1	106.1	193.8
1900	87.9	**206.9**	144.3	124.6	135.8	**214.1**	**220.2**	141.2	123.8	176.9
1910	186.6	154.1	105.5	141.2	**215.9**	137.2	**222.6**	90.6	120.4	**247.0**
1920	163.7	**233.6**	107.4	**204.2**	160.2	84.9	146.0	136.7	119.6	126.1
1930	87.5	135.3	165.3	**207.6**	173.5	178.0	163.1	180.3	174.1	118.8
1940	95.7	151.8	162.3	**201.2**	198.3	133.6	153.4	177.1	**201.5**	137.2
1950	141.7	115.6	111.4	166.3	194.7	**209.6**	163.1	67.9	123.9	**209.7**
1960	124.3	167.3	189.9	128.5	157.6	169.0	189.9	157.5	173.7	139.3
1970	107.0	183.0	160.7	**207.5**	159.2	180.9	157.8	182.7	136.3	85.1
1980	162.3	189.0	126.3	151.7	191.0	154.7	**204.8**	100.5	190.7	74.9
1990	52.1	215.9	**207.2**	102.7	143.0	184.9	193.5	81.2	**249.6**	

References

AISN Software (1999) AutoSignal, version 1.5 for Windows. SPSS Inc. Chicago, IL, USA

Archambault S, Bergeron Y (1992) A 802-year tree-ring chronology from the Québec boreal forest. Can J For Res 5: 674–682

Barlow M, Nigam S, Berbery EH (2001) ENSO, Pacific decadal variability, and U.S. summertime precipitation, drought, and stream flow. J Clim 14: 2105–2128

Barnston AG, Livezey, RE (1987) Classification, seasonality and persistence of low frequency atmospheric circulation patterns. Mon Weather Rev 115: 1083–1126

Bégin Y (2000) Ice-push disturbances in high-Boreal and Subarctic lakeshore ecosystems since AD 1830, northern Québec, Canada. The Holocene 10: 173–183

Bégin Y, Payette S (1988) Dendroecological evidence of lake-level changes during the last three century in subarctic Québec. Quat Res 30: 210–220

Bégin Y, Bérubé D, Grégoire M (1993) Downward migration of coastal conifers as a response to recent land emergence in Hudson Bay, Québec. Quat Res 40: 81–88

Bergeron Y (1991) The influence of island and mainland lakeshore landscapes on boreal forest fire regimes. Ecology 6: 1980–1992

Bergeron Y (1998) Les conséquences des changements climatiques sur la fréquence des feux et la composition forestière au sud-ouest de la forêt boréale québécoise. Géogr Phy Quat 52: 167–173

Bergeron Y (2000) Species and stand dynamics in the mixed woods of Québec's boreal forest. Ecology 81: 1500–1516

Bergeron Y, Archambault S (1993) Decreasing frequency of forest fires in the southern boreal zone of Québec and its relation to global warming since the end of the 'Little Ice Age'. The Holocene 3: 255–259

Bergeron Y, Flannigan MD (1995) Predicting the effects of climate change on fire frequency in the southeastern Canadian boreal forest. Water Air Soil Poll 82: 437–444

Bergeron Y, Gauthier S, Kafka V, Lefort P, Lesieur D (2001) Natural fire frequency for the eastern Canadian boreal forest: consequences for sustainable forestry. Can J For Res 31: 384–391

Biondi F, Gershunov A, Cayan DR (2001) North Pacific decadal climate variability since AD 1661. J Clim 14: 5–10

Bonsal BR, Lawford RG (1999) Teleconnections between El Niño and La Niña events and summer extended dry spells on the Canadian Prairies. Int J Climatol 19: 1445–1458

Bonsal BR, Chakravarti AK, Lawford RG (1993) Teleconnections between North Pacific SST anomalies and growing season extended dry spells on the Canadian Prairies. Int J Climatol 13: 865–878

Bonsal BR, Shabbar A, Higuchi K (2001) Impacts of low frequency variability modes on Canadian winter temperature. Int J Climatol 21: 95–108

Bradley RS (1999) Paleoclimatology: reconstructing climates of the Quaternary. Academic Press, Toronto, Cannada

Charron D, Bergeron Y (2000) Paper birch and trembling aspen chronologies from the Québec boreal forest. Int Conf dendrochronology for the third millennium, Mendoza, Argentina, 2-7 April 2000, pp 10

Cook ER, Holmes R (1986) Guide for computer program ARSTAN. Laboratory of Tree-Ring Research, University of Arizona, Tucson, Arizona, 51 pp

Cook ER, Kairiukstis LA (1990) Methods of dendrochronology. Applications in the environmental sciences. Kluwer Academic Publishers, Boston, pp 408

Cook ER, Peters K (1981) The smoothing spline: a new approach to standarizing forest interior tree-ring width series for dendroclimatic studies. Tree Ring Bull 41: 45–53

Cook ER, Briffa KR, Jones PD (1994) Spatial regression methods in dendroclimatology: a review and comparison of two techniques. Int J Climatol 14: 379–402

Cook ER, D'Arrigo R, Briffa KR (1998) A reconstruction of the North Atlantic Oscillation using tree-ring chronologies from North America and Europe. The Holocene 8: 9–17

D'Arrigo R, Villalba R, Wiles G (2001) Tree-ring estimates of Pacific decadal climate variability. Clim Dyn 18: 219–224

D'Arrigo R, Buckley B, Kaplan S, Woollett J (2002) Interannual to multidecadal modes of Labrador climate variability inferred from tree rings. Clim Dyn 20: 219–228

Ecological Stratification Working Group (1996) A national ecological framework for Canada, Agriculture and Agri-Food Canada and Environment Canada, Ottawa, 125 pp

Environment Canada (2000) Canadian daily climate data: temperature and precipitation. Meteorological Service of Canada. Climate Monitoring and Data Interpretation Division of the Climate Research Branch. Downsview, Ontario, Canada

Environment Canada (2002) Canadian Climate Normals 1971–2000. Canadian Climate Program. Environnement Canada. Atmospheric Environnement Service, Downsview, Ontario, Cannada

Finney B, Gregory-Eaves I, Sweetman J, Douglas M, Smol JP (2000) Impacts of climatic change and fishing on Pacific salmon abundance over the past 300 years. Science 290: 795–799

Flannigan MD, Wotton BM (2001) Climate, weather, and area burned. In: Forest fires, Academic Press, New York, USA pp 351–373

Flannigan MD, Bergeron Y, Englemark O, Wotton BM (1998) Future wildfire in circumboreal forests in relation to global warming. J Veg Sci 9: 469–476

Flannigan MD, Cambell I, Wotton M, Carcaillet C, Richard P, Bergeron Y (2001) Future fire in Canada's boreal forest: paleoecology results and general circulation model – regional climate model simulations. Can J For Res 31: 854–864

Fritts HC (1991) Reconstructing large-scale climatic patterns from tree-ring data-a diagnostic analysis. The University of Arizona Press, Tucson, Ariizona USA pp 286

Fritts HC (2001) Tree-Ring and climate. Blackburn Press, Caldwell, N.J. USA pp 567

Gillett NP, Allen MR, McDonald RE, Senior CA, Shindell DT, Schmidt GA (2002) How linear is the Arctic Oscillation response to greenhouse gases? J Geophys Res 107, ACL 1-1-1-7, 10.1029/2001JD000589

Girardin MP, Tardif J, Bergeron Y (2001) Radial growth analysis of *Larix laricina* from Lake Duparquet area, Québec, in relation to climate and larch sawfly outbreaks. Écoscience 8: 127–138

Girardin MP, Tardif J, Bergeron Y (2002a) Dynamics of eastern larch stands and its relationships with larch sawfly outbreaks in the Northern Clay Belt of Quebec. Can J For Res 32 : 206–216

Girardin MP, Tardif J, Flannigan, MD, Bergeron Y (2002b) Reconstructing atmospheric circulation history using tree rings: one more step toward understanding temporal changes in forest dynamics. In: Veeman TS, Duinker PN, Macnab BJ, Coyne AG, Veeman kM, and Korber D. (eds) Proc 3rd Sustainable Forest Management Network Conference, Advances in forest management: from knowledge to practice, Shaw Conference Centre, Edmonton, Alberta, November 13–15. Edmonton Alberta, Canada, pp 105–110

Girardin MP, Tardif J, Flannigan MD, BM Wotton, Bergeron Y (2004) Trends and periodicities in the Canadian Drought Code and their relationships with atmospheric circulation for southern Canadian boreal forest. Can J For Res 34: 103–119

Glueck MF, Stockton CW (2001) Reconstruction of the North Atlantic Oscillation. Int J Climatol 21: 1453–1465

Hare SR, Mantua NJ (2000) Empirical evidence for North Pacific regime shifts in 1977 and 1989. Prog Oceanogr 47: 103–145

Hofgaard A, Tardif J, Bergeron Y (1999) Dendroclimatic response of *Picea mariana* and *Pinus banksiana* along a latitudinal gradient in the eastern Canadian boreal forest. Can J For Res 29: 1333–1346

Holmes RL (1999) Dendrochronology program library and the dendroecology program library. Laboratory of Tree-Ring Research, University of Arizona, Tucson, Arizona, USA

Holmes RL, Adams RK, Fritts HC (1986) Tree-ring chronologies of western North America: California, eastern Oregon and northern Great Basin with procedures used in chronology development work including users manuals for computer programs COFECHA and ARSTAN. Laboratory of Tree-Ring Research, University of Arizona, Tucson, Arizona, pp 182

Houghton JT, Ding Y, Griggs DJ, Noguer M, Van der Linden PJ, Xiaosu D, Maskell K, Johnson CA (2001) Climate change 2001: the scientific basis. Contribution of Working Group I to the third assessment report of the Intergovernmental Panel on Climate Change (IPCC). Cambridge University Press, Cambridge, UK pp 944

Hurrell JW (1995) Decadal trends in the North Atlantic Oscillation regional temperatures and precipitation. Science 269: 676–679

Hurrell JW (1996) Influence of variations in extratropical wintertime teleconnections on Northern Hemisphere temperatures. Geophys Res Lett 23: 665–668

Hurrell JW, Van Loon H (1997) Decadal variations in climate associated with the North Atlantic Oscillation. Clim Change 36: 301–326

Kalnay E, Kanamitsu M, Kistler R, Collins W, Deaven D, Gandin L, Iredell M, Saha S, White G, Woollen J, Zhu Y, Chelliah M, Ebisuzaki W, Higgins W, Janowiak J, Mo KC, Ropelewski C, Wang J, Leetmaa A, Reynolds R, Jenne R, Joseph D (1996) The NCEP/NCAR reanalysis 40-year project. Bull Am Meteorol Soc 77:437–471

Kiladis GN, Diaz HF (1989) Global climate anomalies associated with extremes in the Southern Oscillation. J Clim 2: 1069–1090

Laprise R, Caya D, Frigon A, Paquin D (2003) Current and perturbed climate as simulated by the second-generation Canadian Regional Climate Model (CRCM-II) over northwestern North America. Clim Dyn 21: 405–421

Latif M, Arpe K, Roeckner E (2000) Oceanic control of decadal North Atlantic sea level pressure variability in winter. Geophys Res Lett 27: 727–730

Lees J, Park J (1995) Multiple taper spectral analysis. Comput Geosci 21: 199

Legendre P, Legendre L (1998) Numerical ecology. Elsevier, New York, pp 853

Luterbacher J, Schmutz C, Gyalistras D, Xoplaki E, Wanner H (1999) Reconstruction of monthly NAO and EU indices back to AD 1675. Geophys Res Lett 26: 2745–2748

Luterbacher J, Xoplaki E, Dietrich D, Rickli R, Jacobeit J, Beck C, Gyalistras D, Schmutz C, Wanner H (2002) Reconstruction of sea level pressure fields over the Eastern North Atlantic and Europe back to 1500. Clim Dyn 18: 545–561

Mantua NJ, Hare SR, Zhang Y, Wallace JM, Francis RC (1997) A Pacific decadal climate oscillation with impacts on salmon. Bull Am Meteorol Soc 78: 1069–1079

McAlpine RS (1990) Seasonal trends in the Drought Code component of the Canadian Forest Fire Weather Index System. For Can, Petawawa National. Forest. Institute, Chalk River, Ont Inf Rep PI-X-97 E/F

Mekis E, Hogg WD (1999) Rehabilitated and analysis of Canadian daily precipitation time series. Atmos-Ocean 37: 53–85

Minobe S (1997) A 50–70 year climatic oscillation over the North Pacific and North America. Geophys Res Lett 24: 683–686

Morin A, Payette S (1984) Expansion récente du mélèze à la limite des for êts (Québec nordique). Can J Bot 62: 1404–1408

Nigam S, Barlow M, Berbery EH (1999) Analysis links Pacific decadal variability to drought and streamflow in the United States. EOS 80: 621–625

Rogers JC (1984) The association between the North Atlantic Oscillation and the Southern Oscillation in the Northern Hemisphere. Mon Weather Rev 112: 1999–2015

Ropelewski CF, Jones PD (1987) An extension of the Tahiti-Darwin Southern Oscillation Index. Mon Weather Rev 115: 2161–2165

Shabbar A, Khandekar M (1996) The impact of El Niño - Southern Oscillation on the temperature field over Canada. Atmos-Ocean 34: 401–416

Shabbar A, Bonsal B, Khandekar M (1997a) Canadian precipitation patterns associated with the Southern Oscillation. J Clim 10: 3016–3027

Shabbar A, Higuchi K, Skinner W, Knox JL (1997b) The association between the BWA index and winter surface temperature variability over eastern Canada and west Greenland. Int J Climatol 17: 1195–1210

Shindell DT, Schmidt GA, Mann ME, Rind D, Waple A (2001a) Solar forcing of regional climate change during the Maunder Minimum. Science 294: 2149–2152

Shindell DT, Schmidt GA, Miller RL, Rind D (2001b) Northern Hemisphere winter climate response to greenhouse gas, ozone, solar, and volcanic forcing. J Geophys Res 106: 7193–7210

Skinner WR, Stocks BJ, Martell DL, Bonsal B, Shabbar A (1999) The association between circulation anomalies in the mid-troposphere and the area burned by wildland fire in Canada. Theo Appl Climatol 63: 89–105

Stahle DW, D'Arrigo R, Krusic PJ, Cleaveland MK, Cook ER, Allan RJ, Cole JE, Dunbar RB, Therrell MD, Gay DA, Moore MD, Stokes MA, Burns BT, Villanueva-Diaz J, Thompson LG (1998) Experimental dendroclimatic reconstruction of the Southern Oscillation. Bull Am Meteorol Soc 79: 2137–2152

Stokes MA, Smiley TL (1996) An introduction to tree-ring dating. University of Arizona Press, Tucson, Arizona, pp 73

Tardif J, Bergeron Y (1997a) Ice-flood history reconstructed with tree-rings from the southern boreal forest limit, western Québec. The Holocene 7: 291–300

Tardif J, Bergeron Y (1997b) Comparative dendroclimatological analysis of two black ash and two white cedar populations from contrasting sites in the Lake Duparquet region, northwestern Québec. Can J For Res 27: 108–116

Tardif J, Bergeron Y (1999) Population dynamics of *Fraxinus nigra* in response to flood-level variations, in northwestern Québec. Ecol Monogr 69: 107–125

Tardif J, Camarero JJ, Ribas M, Gutiérrez E (2003) Spatiotemporal variability in tree growth in the Central Pyrenees: climatic and site influences. Ecol Monogr 73: 241–257

Ter Braak CJF (1994) Canonical community ordination. Part I: basic theory and linear methods. Écoscience 1: 127–140

Ter Braak CJF, Prentice IC (1988) A theory of gradient analysis. Adv Ecol Res 18: 271–317

Ter Braak CJF, Smilauer P (1998) Canoco reference manual and user's guide to Canoco for windows: software for canonical community ordination (version 4). Microcomputer power, Ithaca, NY, USA, pp 325

Thompson DWJ, Wallace JM (1998) The Arctic Oscillation signature in the wintertime geopotential height and temperature fields. Geophys Res Lett 25: 1297–1300

Thompson DWJ, Wallace JM (2001) Regional climate impacts of the Northern Hemisphere annular mode. Science 293: 85–89

Thornthwaite CW, Mather JR (1955) The water balance. Publ Climatol 8: 1–86

Torrence C, Compo GP (1998) A practical guide to wavelet analysis. Bull Am Meteorol Soc 79: 61–78

Torrence T, Webster PJ (1999) Interdecadal changes in the ENSO-Monsoon System. J Clim 12: 2679–2690

Turner JA (1972) The drought code component of the Canadian Forest Fire Behaviour System. Env Can, Can For Serv, Ottawa, Ontario, Pub 1316, pp 14

Van Wagner CE (1970) New development in forest fire danger rating. Canada Department of Fisheries Forestry Canadian Forest Service Information Report PS-X-19

Van Wagner CE (1987) Development and structure of the Canadian Forest Fire Weather Index System. Cannadian Forest Service, Ottawa, Ontario, For Tech Rep. 35, pp 37

Varem-Sanders T (2000) ITRVIEW 2.0 program. Canadian Forest Service, Edmonton, Alberta, Cannada

Vincent LA (1998) A technique for the identification of inhomogeneities in Canadian temperature series. J Clim 11: 1094–1104

Vincent LA, Gullett DW (1999) Canadian historical and homogeneous temperature datasets for climate change analyses. Int J Climatol 19: 1375–1388

Vincent JS, Hardy L (1977) L'évolution et l'extinction des lacs glaciaires Barlow et Ojibway en territoire québécois. Géogr Phy Quat 31: 357–372

Wanner H, Brönnimann S, Casty C, Gyalistras D, Luterbacher J, Schmutz C, Stephenson DB, Xoplaki F (2001) North Atlantic Oscillation – concepts and studies. Surv in Geophys 22: 321–382

Zhang Y, Wallace JM, Battisti DS (1997) ENSO-like interdecadal variability: 1900–93. J Clim 10: 1004–1020

Zhang X, Vincent L, Hogg WD, Niitsoo A (2000) Temperature and precipitation trends in Canada during the 20th century. Atmos-Ocean 38: 395–429

Zheng D, Chao BF, Zhou Y, Yu N (2000) Improvement of edge effect of the wavelet time-frequency spectrum: application to the length-of-day series. J Geodesy 74: 249–254